Orbit Analysis For Imbalance Fault Detection In Rotating Machinery

Cesar Da Costa[1]*, Ronaldo S. Da Gama[1], Carlos E. Nascimento[1], Iago M. Brandão[1], Everton C. De Medeiros[2], Mauro H. Mathias[2]

[1]Department of Control and Automation Engineering, IFSP-Federal Institute of São Paulo, SP, 01109-010, Brazil
[2]Department of Mechanical, UNESP- State University of São Paulo Julio de Mesquita Filho, SP, 12516-410 , Brazil
Corresponding author:Cesar da Costa

Abstract: *Analysis of the axis orbit is extremely important for monitoring faults in rotary machines and making an associated diagnosis for repair. The development of both experimental procedures based on implementation of instrumentation systems and computational tools applied in the treatment and monitoring of dynamic quantities that describe the behavior of machines under operating conditions are of fundamental importance in the design and maintenance of rotating induction machines. The aim of this present work is to develop an experimental setup for studying and testing the technique of orbit analysis using analytical, numerical, and experimental methods. An experimental theoretical study on the concept of orbit analysis is presented; this can be applied to diagnose faults in rotary induction machines, such as turbines and turbochargers within petrochemical industries. Experimental results subsequently validate the proposed system.*
Keywords:*three-phase induction machine; misalignment; diagnosis; experimental tests*

I. Introduction

Monitoring the state of rotary induction machines and diagnosing incipient faults is necessary to increase the reliability of productive systems [1, 2]. The axis orbit is one of the most important focuses when conduction vibration analysis on a rotating machine, and different axis orbits reflect various running states and provide rotor failure information. However, traditional methods used to identify the axis orbit have serious fault diagnosis limits on an automation level [3, 4]. The orbit diagram is a graphical tool for monitoring the orbit and is described by the center of the machine's axis along its radial plane. The orbit is plotted using the alternate current level of the quadrature proximity sensors [5,6]. Orbital analysis [7] focuses on the trajectory of the center of the axis in the reading plane of a pair of proximity sensors that are mounted rigidly on the machine's frame together with shaft support zones (bearings). Thus, the orbit represents the trajectory of the center of the axis relative to the structure of the machine. The graph is easy to interpret and provides adequate information about the orbit for use in effectively diagnosing rotating machine malfunctions [8].The study and definition of rotor dynamics parameters, such as critical speeds, their response to imbalanced forces, and the influence of bearing damping, are vital in the design of rotating machines. An experimental simulation platform is usually employed to experimentally validate proposed systems, and in this respect, Shakya et al. [1] applied several types of proximity sensors to monitor the condition of a machine to increase the reliability of diagnosis.The study of orbit analysis in three-phase induction machines has attracted considerable research attention. For example, Yang et al. [4] proposed an orbit analysis using an analysis and comparison of 22 characteristics of the axis orbit for online fault pattern recognition; simulated results showed the potential of this strategy. In addition, Hongxin et al. [9] implemented a fault-diagnosis system to measure and analyze orbits on axes using LabVIEW software, and Kelm and Pavelek [8] reported that orbit analysis represents the trajectory of the center of the axis in the reading plane of a pair of proximity sensors.Using software and hardware systems, a flexible rotor experimental setup, and a data acquisition system, this work contributes to the measurement and recognition of shaft orbits. In this study, a smart experimental setup is developed that involves a field programmable gate array (FPGA)-based signal processor with parallel architecture for multiple-signal processing that combines shaft orbits and Fast Fourier Transform (FFT) analysis.This paper is organized as follows. Section 2 provides a brief description of vibration analysis and orbit analysis; Section 3 presents mathematical modeling of a rigid-shaft rotor and flexible bearings; Section 4 illustrates the proposed methodology; Section 5 presents results of the experimental rotor kit; and the conclusion is provided in Section 6.

II. Background

2.1 Vibration analysis

Vibration analysis is applied to rotating equipment, such as gas turbines, pumps, motors, compressors, papermaking machines, or gearboxes, and is used to determine the mechanical, electrical, and operating condition of the equipment. The main advantage of this type of analysis is that problems can be identified before they become critical, and analysis can be conducted using continuous monitoring (online or wireless) or at scheduled intervals (offline) through manual collection. A vibration analysis system generally contains four components: (i) sensors for data collection that are usually of an accelerometer type; (ii) a signal analyzer; (iii) compatible software; and (iv) a computer for data analysis and storage. These components can be configured to form an offline, online, or wireless system [10, 11].Vibration monitoring can detect defects, for example with bearings at various stages of deterioration, or misalignment, imbalance, mechanical gaps, broken gears, or teeth. Such defects can be detected by analyzing the trend curve of the vibration amplitude. After the problem has been detected, a spectral analysis can be conducted to precisely define presenting issues and to estimate the length of time the machine will continue to operate prior to failure [12,13].

2.2 Orbit analysis

The time signal provides important and useful information; however, if the axis only moves on a two-dimensional path, the information obtained is limited [14]. To monitor such movement, one sensor needs to be installed perpendicular to the second sensor, and an inductive proximity sensor is generally used in this respect. After installing the second sensor, certain conditions need to be met to determine the movement of the center of the axis in this plane. This information obtained can be presented using two individual time signals, respectively, for each sensor, but ideally a graph can be drawn that represents the two dimensions of the axis' movement [15]. This is the purpose of the orbit. Figure 1 shows the assembly scheme of inductive proximity sensors used in orbital analysis.
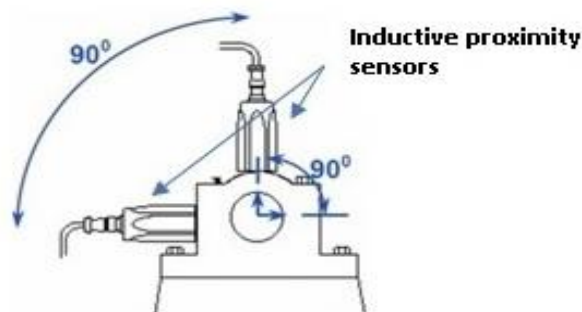

Fig. 1. Schematic of assembly of inductive proximity sensors.

The orbit [4] represents the trajectory of the center of the axis of a pair of proximity sensors in a reading plane. The lateral vibration signals of the rotor indicate oscillating movements of the shaft in one direction only, but when a sensor is positioned perpendicular to the other, it is possible to follow the two-dimensional movement of the vibration by looking at the path along which the center of the rotor moves. This movement in a plane is known as the orbital motion of the rotor [9]. The orbit of a rotor represents the path of the centerline of a given axis relative to the pair of perpendicular sensors installed therein. In addition to the orbit obtained experimentally, numerical modeling enables visualization of these orbits at a given rotation and position of the rotor, as well as with the modes of vibration [4, 8, 9, 14]. Figure 2 shows the progression of the center of the axis around its orbit from points 1 to 5.
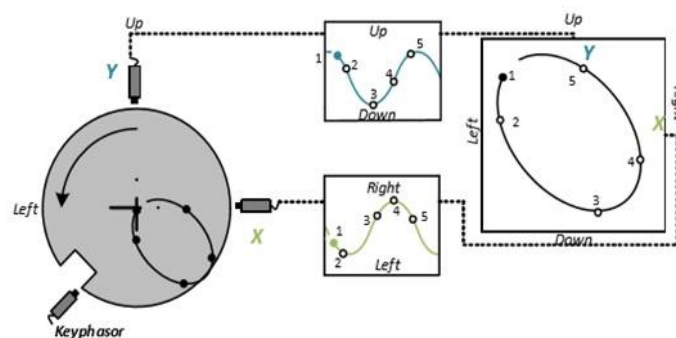

Fig. 2. Orbit resulting from pair of XY sensors.

III. Mathematical modeling

A mathematical model can be used to describe the behavior of a rotating machine that rotates around its axial axis and is supported at its ends by bearings. In mathematical modeling, the behavior of the system is translated into the language of mathematics, and computerscanbeusedtoperformnumericalcalculations. According to Friswell et al. [16], a model that uses a formulation with Newton's Laws for a rigid-shaft rotor and flexible bearings contributes to our understanding of rotor behavior by including or removing some boundary conditions, such as the gyroscopic effect and rigidity behavior within the system. When solving problems considering the gyroscopic effect and anisotropy in bearings (a bearing with different stiffness behavior in different directions), it is difficult to determine the orbit of movement of the axis because of the differences in properties in the x- and y-direction (the orbit has an elliptical shape). In addition, in rotors with anisotropic bearings, the precession of the shaft has two behaviors, forward and reverse precessions, where forward precession is the movement relating to lateral vibration of the axis accompanying the same direction of rotation, and reverse precession occurs in the opposite direction.Considering that the rotor is uniform and that it rotates at a constant rotation, Ω, on the axis, Oz, the equations of motion can be formulated by considering a general case, such as a rotor with a disc that is not centered on the axis (Figure 3), has different stiffness bearings, and includes the gyroscope effect.
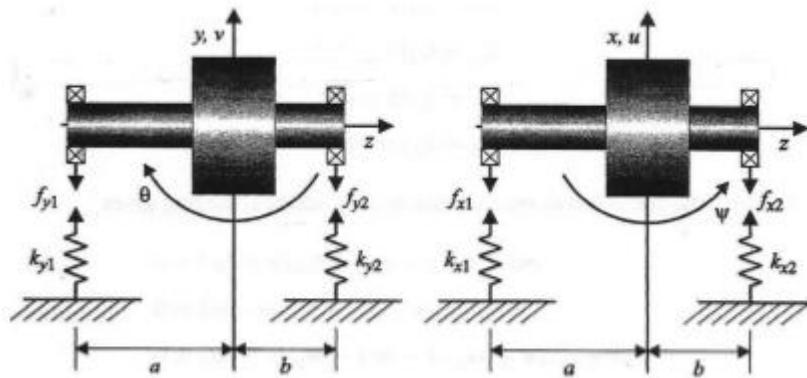

Fig. 3. Free-body diagram for rigid rotor in flexible bearings.

Applying Newton's second law for the free rotor of external excitation, we obtain

$$\sum F_x \Rightarrow -f_{x1} - f_{x2} = m\ddot{u} \tag{1}$$

$$\sum F_y \Rightarrow -f_{y1} - f_{y2} = m\ddot{v} \tag{2}$$

$$\sum M_\theta \Rightarrow -af_{y1} - bf_{y2} = I_d\ddot{\theta} + I_p\Omega\dot{\psi} \tag{3}$$

$$\sum M_\psi \Rightarrow -af_{x1} - bf_{x2} = I_d\ddot{\psi} + I_p\Omega\dot{\theta} \tag{4}$$

Assuming that the values of forces obey Hooke's Law, where in each directionthere is a stiffness value, k, the equations of motion for the rigid rotor will be

$$m\ddot{u} + (k_{x1} + k_{x2})u + (-ak_{x1} + bk_{x2})\psi = 0 \tag{5}$$

$$m\ddot{v} + (k_{y1} + k_{y2})v + (ak_{y1} - bk_{y2})\theta = 0 \tag{6}$$

$$I_d\ddot{\theta} + I_p\Omega\dot{\psi} + (ak_{y1} - bk_{y2})v + (a^2k_{y1} + b^2k_{y2})\theta = 0 \tag{7}$$

$$I_d\ddot{\psi} - I_p\Omega\dot{\theta} + (-ak_{x1} + bk_{x2})u + (a^2k_{x1} + b^2k_{x2})\psi = 0 \tag{8}$$

By grouping the stiffness values (k) as translational (Eq. 9 and 12), coupled (Eq. 10 and 13), and rotational, (Eq. 11 and 14) can be expressed as follows,

$$k_{xT} = k_{x1} + k_{x2} \tag{9}$$

$$k_{xC} = -ak_{x1} + bk_{x2} \quad (10)$$

$$k_{xR} = a^2k_{x1} + b^2k_{x2} \quad (11)$$

$$k_{yT} = k_{y1} + k_{y2} \quad (12)$$

$$k_{yC} = -ak_{y1} + bk_{y2} \quad (13)$$

$$k_{yR} = a^2k_{y1} + b^2k_{y2} \quad (14)$$

Therefore, general-motion equations can be written more concisely by substituting Equations 9–14 into Equations 5–8. The system formed by Equations 15–18 thus describes the dynamic behavior of the rotating machine studied in this work and are presented as follows

$$m\ddot{u} + k_{xT}u + k_{xC}\psi = 0, \tag{15}$$

$$m\ddot{v} + k_{yT}v - k_{yC}\theta = 0, \tag{16}$$

$$I_d\ddot{\theta} + I_p\Omega\dot{\psi} - k_{yC}v + k_{yR}\theta = 0, \tag{17}$$

$$I_d\ddot{\psi} - I_p\Omega\dot{\theta} + k_{xC}u + k_{xR}\psi = 0. \tag{18}$$

IV. Proposed methodology

In this study, the authors investigate the dynamic behavior in rotary induction machines using computational analysis and experimental results obtained on a test bench. This study is divided into two phases: construction of a mathematical model and use of experimental methods.

4.1 Mathematical model

The model used for mathematical modeling is the Jeffcott Rotor (Figure 4), which consists of an imbalanced disc located in the middle of an axis of mass that rotates around its axial axis that is supported at its ends by bearings [17, 18]. Despite the simplicity of the model, it enables us to observe and improve our understanding of many common phenomena relating to rotary machines dynamics, such as critical velocities and the influence of viscous resistances on stability. Several considerations are made for this model, which is constructed using the finite element method, to better-approximate the experimental results and thus validate the mathematical model. Use of experiments for validating theoretical and numerical models is important for studying the dynamic behavior of rotary machines.

The Jeffcott Rotor model with a central disc was modeled using MATLAB/Simulink software, according to Equations 15 to 18. The following figures present graphs of the modeling: Figure 5a shows simulated deformation imposed on the Y-axis by imbalance, and Figure 5b shows that typical axis X and Y orbits can be simulated by adjusting the parameters of the mathematical model.
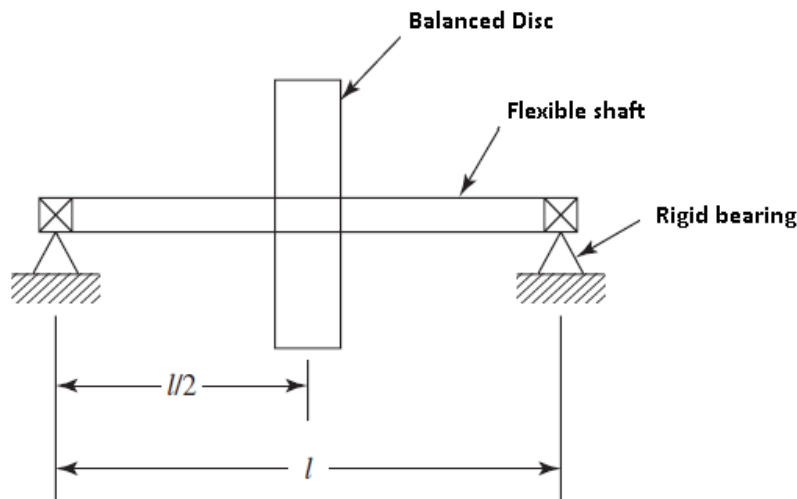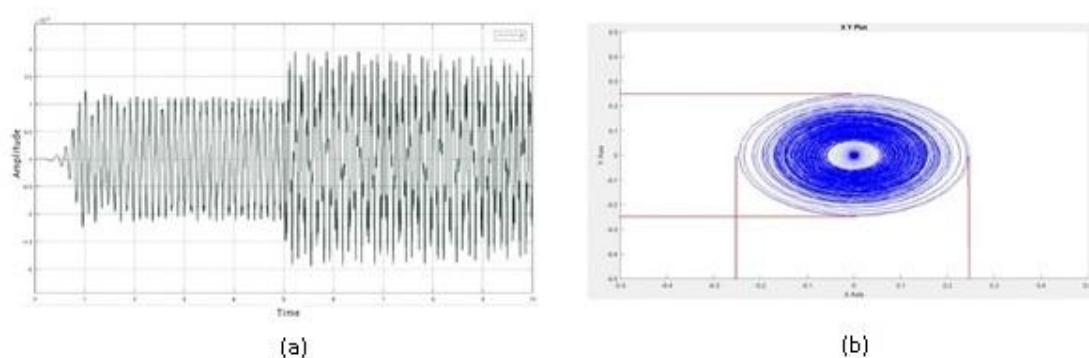

Fig. 4. Jeffcott Rotor with central disk.

Fig. 5. Imbalanced simulated Y-axis (a) and Simulated XY orbit (b).

4.2 *Experimental procedure*

An experiment was conducted using an experimental rotor kit developed by the authors that was interconnected to a FPGA based computer system. The rotor kit has two pairs of proximity sensors rigidly installed near the shaft. To introduce imbalance, the rotor kit has a disc coupled to the shaft in which imbalance weights are inserted. Figure 6 schematizes both the rotor kit components and the computational part.
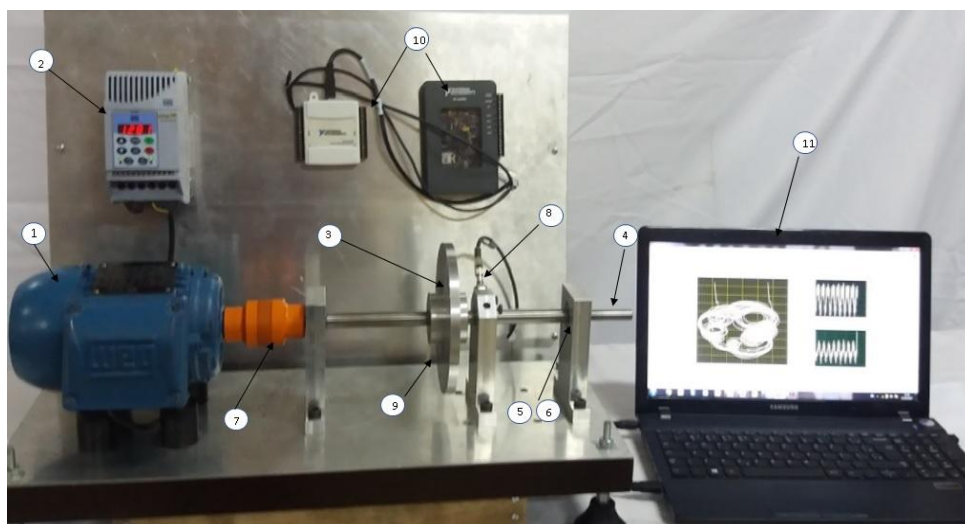

Fig. 6. Experimental setup.

1. 3-phase induction motor (220/380V, 0.25 cv, 4 poles, 1710 rpm);
2. Variable speed controller with voltage vector control;
3. Experimental rotor kit consisting of one disc measuring 160 mm in diameter and 16 mm in thickness, into which holes were punched to introduce imbalance;
4. Rectified shaft 16 mm in diameter and 255 mm in length;
5. Rolling bearings;
6. Ball bearings, with a reference frequency of 38,000 rpm and dynamic load of 351 kgf;
7. Helical coupling, allowing an angular misalignment of 5° at a reference frequency of 25,000 rpm and rated torque of 2.3 Nm;
8. Two proximity sensors eddy current (model IWRM, manufacturer Baumer);
9. Photoelectric sensor to generate the trigger signal;
10. Data acquisition and processor MyRIO (hardware architecture) with real-time processor and FPGA chip;
11. PC running application software in LabVIEW.

4.3 *Proposed algorithm embedded in FPGA*

The algorithm consists of several modules (which include data acquisition and fault detection) to enable drawing of the shaft orbit graph, calculation of FFT, and a full spectrum analysis. A block diagram of the algorithm embedded in the FPGA is shown in Figure 7. The full spectrum is calculated by applying the FFT algorithm to the waveform of each sensor. Results are then subjected to another transform, which converts the data into two new spectra representing precession frequencies: a precession spectrum X for Y and a precession

Y for X. Finally, the direction of rotation is used to determine which of the spectra represents the forward precession frequencies, and which represents the reverse precession frequencies. When this process is completed, the two spectra are combined in a single graph.
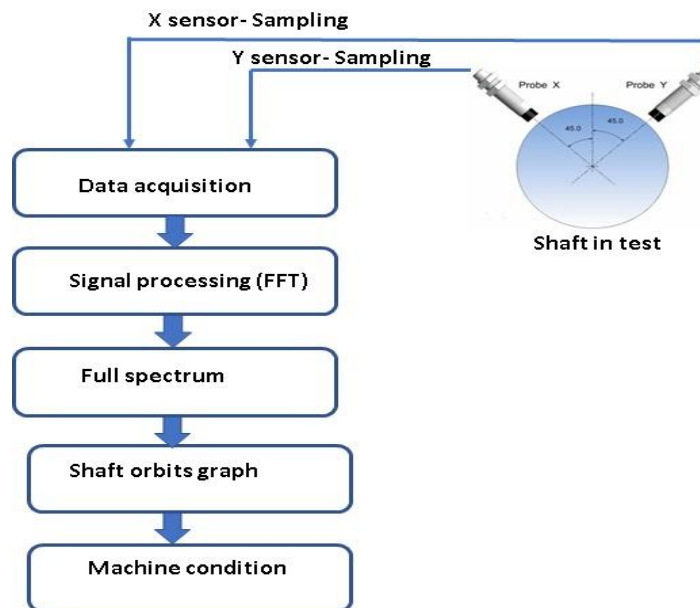

Fig. 7. Experimental setup.

4.4 Data processing

The hardware platform myRIO is based on FPGA technology, and the NI myRIO 1900 model was used to acquire and process the signals obtained from the experimental setup, perform data acquisition and analysis, and process essential calculations for the mathematical application software. The physical interface with sensors served as the real-time operating system and was used to condition the signal. The myRIO hardware architecture combines two components: a real-time processor as the system CPU and a FPGA chip embedded in the structure. A measurement system based on LabVIEW software was made of eddy current sensors (x-y axis), a pre-amplifier, low-pass filter, and NI card myRIO 1900, as shown in Figure 8.
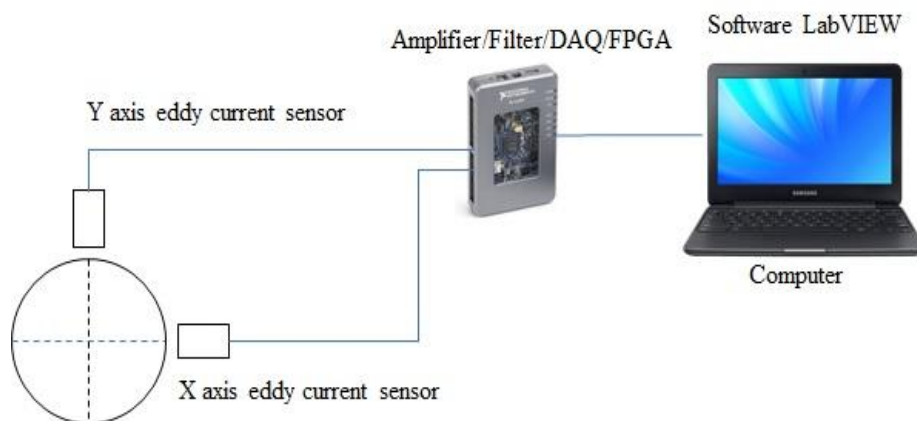

Fig.8. Block diagram of shaft orbits measurement system.

The algorithms used for data acquisition, signal processing, full spectrum analysis, the shaft orbit graph, and fault detection were developed using LabVIEW software. To verify faults and confirm accuracy of results, a spectrum analysis control panel interface was developed, as shown in Figure 9. The ellipse curve on the right side of the control panel is the shaft orbit measurement, and the graphs on the left side represent the single-channel radial displacement and its spectrum, respectively. A characteristic orbit format exists for the main failure types, and the correlation between the theoretical orbit format and the orbit reproduced in the developed experimental setup was verified in practice.
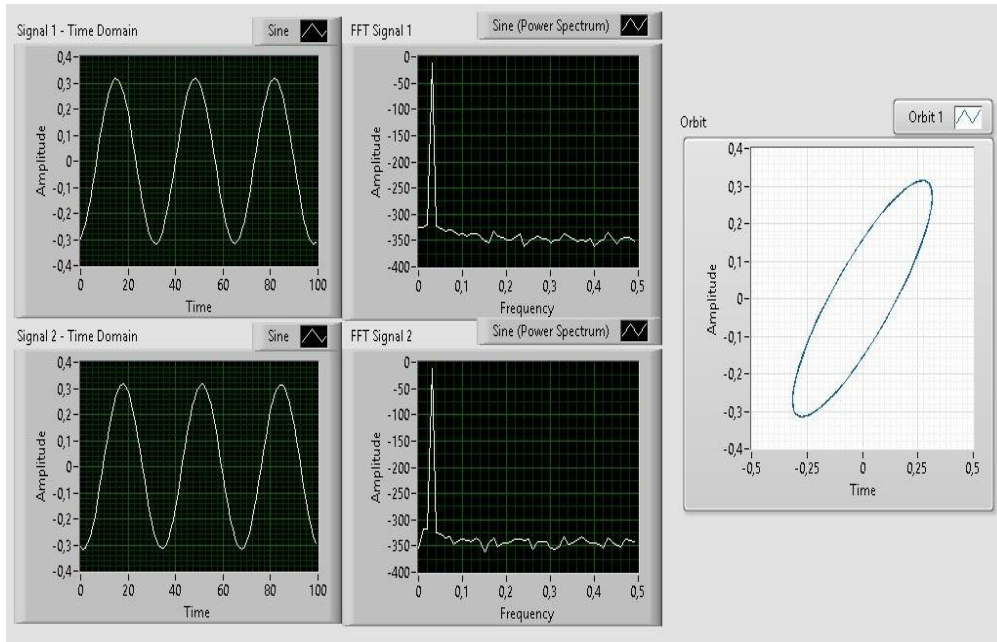
Fig. 9. Developed system control panel.

V. Results and analysis

A model of the experimental rotor kit used to conduct orbit analysis and determine dynamic behavior was designed in analogy to the equipment used in the industrial environment. The experimental rotor kit in this study represents a combination of rotary machines found in industrial applications, such as compressors, turbo-compressors, turbines, and centrifugal pumps. The differences between machines relates to the amount of elements that make up the rotor, such as the number of bearings, number of impellers (simulated through discs), and any changes in the foundation types and geometry of the systems. Creo Parametric 3D modeling software (Figure 10) was used to design the experimental rotor kit, both for the elements and to manufacture design drawings.
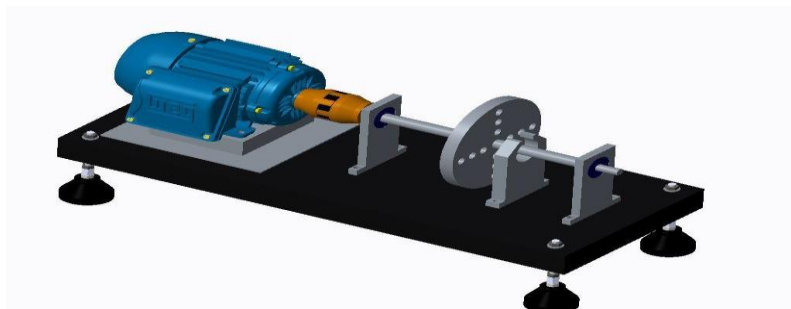

Fig. 10.3D rotor kit design.

The experimental rotor kit was mounted with a centered disc using a steel shaft; this type of assembly is similar to the rotor model proposed by Jeffcott, as illustrated in Figure 4. Table 1 shows the dimensions and characteristics of the rotor kit used in experimental tests.

Table 1: Parameters of rotor kit

	Shaft	*Disc*
Density [kg/m^3]	7810	7810
ϕ (outer) [mm]	16,00	160,00
ϕ (inner) [mm]	0,00	16,00
Length [mm]	255,00	16,00
$I_p[kgm^2]$	$6,1\times10^{-5}$	0,0236
$I_d[kgm^2]$	0,0256	0,0118

5.1 Machine running balanced

Figure 11 shows results obtained from data collected. The orbit provides all the information required with respect to the theoretical basis presented in this work, in relation to rotation, precession, and for the orbit's profile. An analysis of the orbit (Figure 11b) shows that it is not perfectly circular. Figure 11a (full spectrum) shows that the 1X reverse component (3,21 μm) is greatly reduced compared to the 1X forward (19.25 μm). Theoretically, when the rotor kit is not under any imbalance or type of defect it should produce a circular profile orbit. Therefore, in the case presented here, the composition of the disc is not uniform, despite the proficiency of the manufacturing process, and the material is not homogeneous; therefore, residual imbalances are introduced.
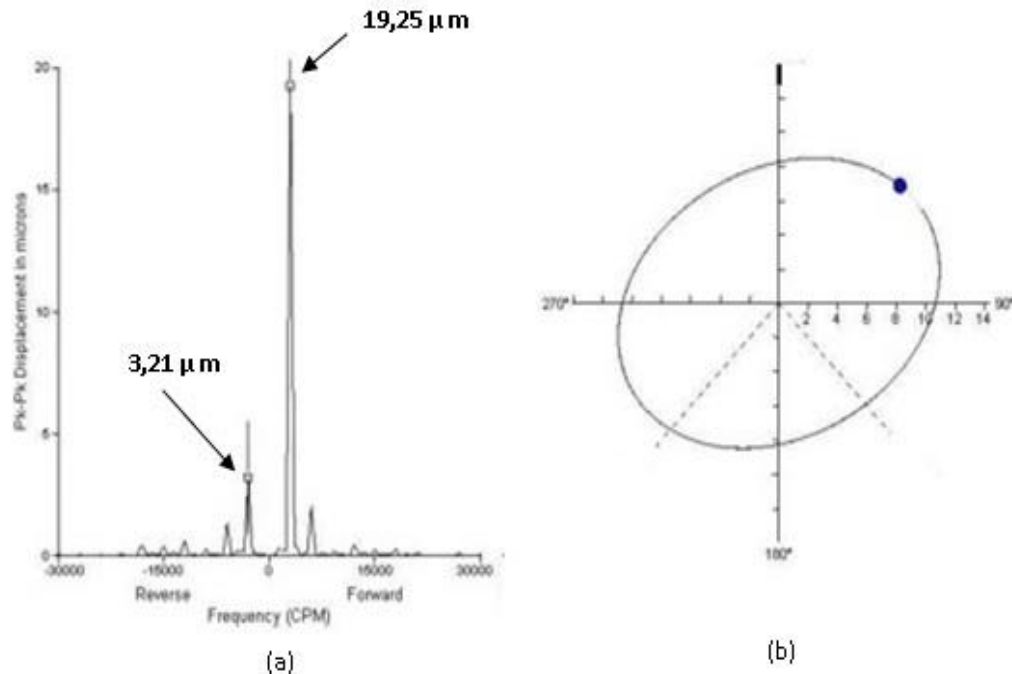
Fig.11. Full spectrum (a) and orbit graph balanced machine (b).

5.2 Machine running imbalanced

The disc from the rotor kit was used to study imbalance. To perform a simulation of imbalance, a trial mass with a pre-determined weight was introduced. The disc (Figure 12) is 160 mm in diameter, has a thickness of 16 mm, consists of 8 M5 holes. Trials were initiated using an unbalanced mass of 2.3 g.
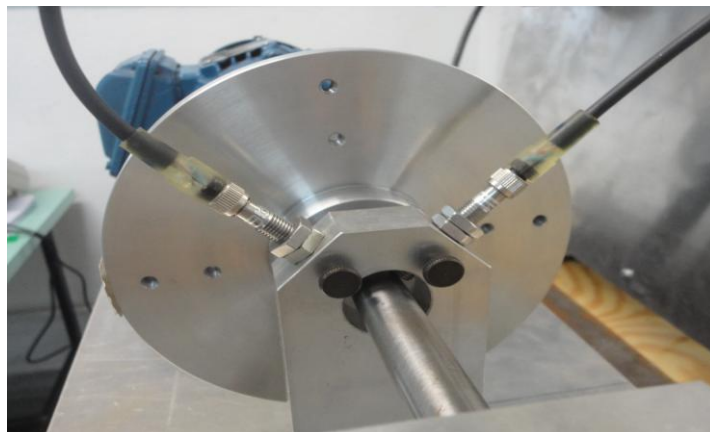
Fig. 12. Imbalance input disc.

Figure 13 shows the successive waveform changes occurring from the moment the kit rotor was stopped when the 2.3 g mass was introduced. A comparison between these results and the reference results of the rotor kit presented in Figure 11, shows that a considerable increase in the 1X forward component occurred (from 19.25 to

73.42 μm) and that this increase was also recorded at 1X reverse (3,211 to 18,55 μm). These results are evidence that the profile of the orbit (Figure 13 b) became slightly more elliptical.
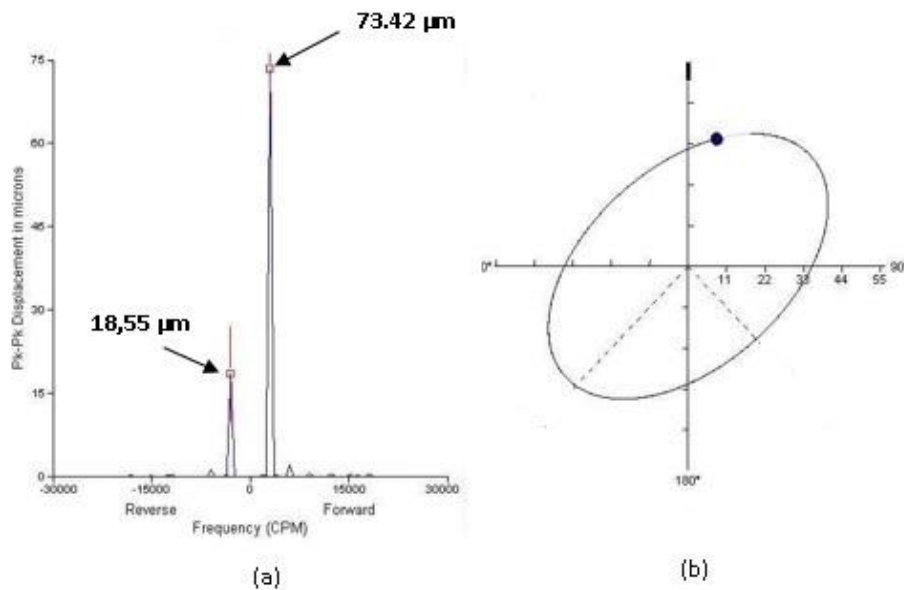

Fig. 13. Full spectrum (a) and orbit graph imbalanced machine (b).

5.3 Applied radial load and misalignment

The second largest problem with rotating machines is the high temperatures recorded on bearings; these are almost always related to high dynamic or static radial loads that may result from the rotor's own weight, mechanical aspects (such as coupling defects), imbalances, or misalignment. With respect to misalignment, the orbits and their respective full spectra behave as follows as the severity of misalignment increases: the 1X and 2X forward components decrease, the 1X and 2X reverse components increase, and the profile of the filtered orbit at 1X finally adopts a pronounced elliptical profile. In this experiment, an angular misalignment was introduced into the rotor kit by introducing a 0.05 mm calibrated wedge.

A comparison of the results presented in Figure 14 with the reference results in Figure 11, shows that there was an increase in the 1X forward component (19.25 to 21.63 μm) and a considerable increase in the reverse component (3.211 to 10.11 μm). It is therefore evident that the main symptom indicative of misalignment is the ellipticity of the profile adopted by the orbit. This can be accordingly seen in the presence and growth of the 1X reverse component; in addition, harmonics 2X and 3X of the speed of rotation (reverse and forward) appear. Figure 15 shows the unfiltered orbit under the same conditions.
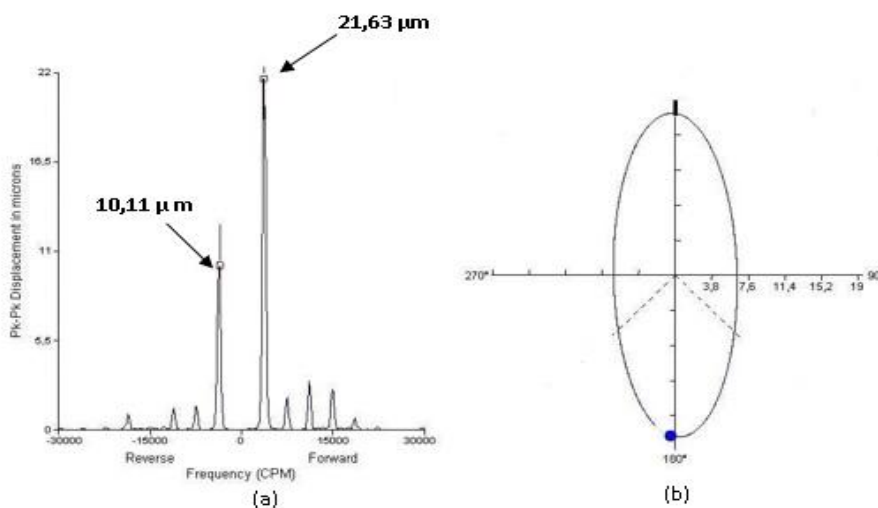

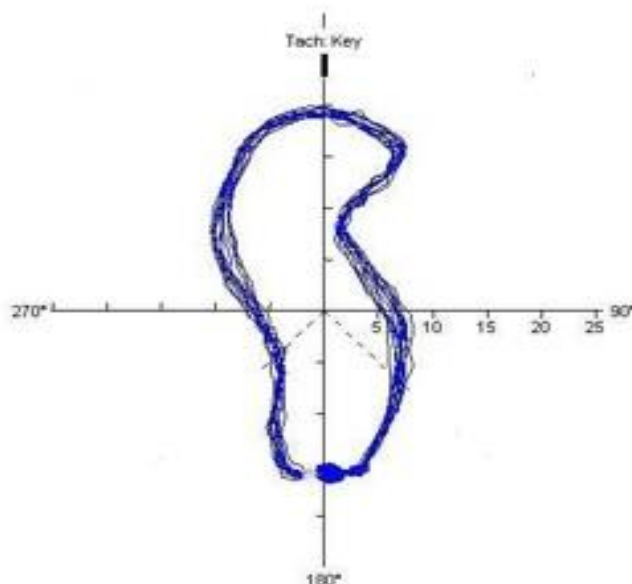**Fig. 13**. Full spectrum (a) and orbit graph misalignment machine (b).

Fig. 15. Unfiltered orbit graph misalignment machine.

VI. Conclusions

The main function of quadrature proximity sensor pairs is to determine the orbit of the machine axis. In this study, the peak-to-peak values of the signals of each proximity sensor were monitored to determine oscillation of the axis. Peaks were detected correctly using a filtered signal, and it was possible to trace the orbit described by the axis. A full spectral analysis of the signals of the proximity sensors was conducted separately for each signal by applying FFT. However, the most complete diagnosis was made by analyzing the spectrum of the orbit recorded with both sensors. The frequency spectrum of the recorded orbit showed consistent results, and it was thus possible to verify that the spectrum is correlated with the behavior recorded by the proximity sensor signals. The largest contributions of this research are providing the possibility of monitoring specific frequencies over time and correlating the changes occurring in certain frequencies with faults (for example an axis unbalance). Furthermore, in addition to detecting changes in operating conditions, this study enables identification of the type of fault likely to have occurred by analyzing the altered pattern of the components of the orbit spectrum analyzed.

References

[1] P. Shakya, A. K. Darpe, M. S. Kulkami, Bearing Diagnosis Using Proximity Probe and Accelerometer. Measurement, v. 80, pp. 190-200, 2016.

[2] N. Bachschmid, P. Pennacchi, A. Vania, Diagnostic significance of orbit shape analysis and its application to improve machine fault detection. Journal of the Brazilian Society of Mechanical Sciences and Engineering, v. 26, n. 2, p. 200-208, 2004.

[3] J. J. Carbajal-Hernandez, L. P. Sanchez-Fernandez, I. Hernandez-Bautista, J. J. Medel-Juarez, L. a. Sanchez, Classification of unbalance and misalignment in induction motors using orbital analysis and associative memories. Neurocomputing, v. 175, p. 838-850, 2016.

[4] L. Yang, J. Wang, G. Zhang, Z. Ding., Analysis and comparison of axis orbit characteristics in fault pattern recognition.2015 Chinese Automation Congress (CAC), p. 859-863, 2015.

[5] M. L. Adams, Rotating Machinery Vibration from Analysis to troubleshooting. Nova York: Marcel Dekker, Inc., 2001.

[6] R. C. Eisenmann, R. Eisenmann Jr., Machinery Malfunction Diagnosis and Correction. Texas: Pearson Education, Inc., 2005.

[7] D. E. Bently, Fundamentals of Rotating Machinery Diagnostics. Minden: Bently Pressurized Bearing Press, 2002.

[8] R. D. Kelm, D. Pavelek, Orbit Analysis. Vibration Institute Annual Training Seminar, p. 1-16, 2012.

[9] Z. Hongxin, Z. Hao, G. Xinpig, M. Teng, H. Xinyu, Y. Yu, Study onshaft orbits measurement and identification based on LabVIEW, 2013 Fifth Conference on Measuring Technology and Mechatronics Automation, p. 1087-1090, 2013.

[10] H. Henao, C. Bruzzese, E. Strangas, R. Pusca, J. Estima, M. Rieraguasp, S. H. Kia, Trends in Fault Diagnosis for Electrical Machines: A Review of Diagnostic Techniques, IEEE Ind. Electron. Mag. V. 8, p.31-42, 2014.

[11] A. Naha, A. K. Samanta, A. Routray, A. K. Deb, A method for detecting half-broken rotor bar in lightly loaded induction motors using current, IEEE Transactions on Instrumentation and Measurement, Vol. 65, p.1614-1625, 2016.

[12]   E. H. Bouchikhi, V. Choqueuse, M. Benbouzid, Induction machine faults detection using stator current parametric spectral estimation, Mech. Syst. Signal Process. Vol. 52, p. 447-464, 2015.

[13]   K. Agoston, Fault detection of the electrical motors based on vibration analysis. Procedia Technology, vol. 19, p. 547-553, 2015.

[14]   M. Monte, F. Verbelen, B. Vervisch, Detection of coupling misalignment by extended orbits. In: Experimental Techniques, Rotating Machinery, and Acoustics, Vol. 8, p. 243-250, 2015.

[15]   N., Littrell, A., Bell, Application Considerations for Eddy Current Proximity Probes. ORBIT Magazine Vol.29, No.1, p. 44-52, 2009.

[16]   M. I., Friswell, J. E. T., Penny, S. D., Garvey, A. W., Lees, Dynamics of rotating machines. 1st ed. New York: Cambridge University Press, 2010. ISBN: 978-0521850162.

[17]   J. P. Chavez, V. V. Hamaneh, M. Wiercigroch, Modelling and experimental verification of an asymmetric Jeffcott rotor with radial clearance. Journal of Sound and Vibration, Vol. 334, p.86-97, 2015.

[18]   G. K. Yamoto, C., Da Costa, J.S.S, Souza, A smart experimental setup for vibration measurement and imbalance fault detection in rotating machinery. Case Studies in Mechanical Systems and Signal Processing, vol. 4, p. 8-18, 2016.